Int. J. Advanced Design and Manufacturing Technology, 2025, Vol. 18, No. 2, pp. 59-69

DOI: 10.71644/admt.2025.1186819 *ISSN: 2252-0406* *https://admt.isfahan.iau.ir*

Effect of Damping and Apparent Resistance on Energy Harvesting from Piezoelectric Beam using Dynamic Stiffness Method

Majid Jabbari[1,*], Bijan Ahmadi[2], Sajad Hamedi[3]
Department of Mechanical Engineering, Khomeinishahr Branch, Islamic Azad University, Khomeinishahr, Isfahan, Iran
E-mail: jabbari@iaukhsh.ac.ir
*Corresponding author

Received: 13 October 2024, Revised: 15 December 2024, Accepted: 7 January 2025

Abstract: There are different sources of energy in the environment, and one of the sources that is converted into electrical energy is the vibrations of the environment. One of the methods of energy extraction is the use of piezoelectric materials. The main advantage of piezoelectric materials is their high-power density and ease of use. In this study, a dynamic stiffness method is developed to extract energy from the piezoelectric cantilever beam despite damping, impedance, and concentrated mass. In order to get the maximum energy for concentrated mass, it is suggested that the effect of some parameters on the proposed system be investigated. Such parameters include damping and impedance effects noted. According to this study, the effect of Kelvin-Voigt damping on the voltage amplitude of the initial acceleration at the first resonant frequency is almost linear, while this value changes homographically at the second resonant frequency. The change in voltage amplitude over the base acceleration amplitude due to the change in the viscous damping coefficient at the first and second resonant frequencies is almost the same, but the amount of reduction is greater in the second case. Also, the effect of impedance on this system is investigated, and the system response is obtained using the dynamic stiffness method. The effect of increasing the impedance on the conductivity of the beam tip relative to the foundation support is such that as impedance increases, its natural frequencies increase, thus making the system more rigid.

Keywords: Damping, Dynamic Stiffness, Energy Harvesting, Piezoelectric Beam

Biographical notes: Majid Jabbari is an assistant professor at the Department of Mechanical Engineering in Islamic Azad University, Khomeinishahr Branch. He received his PhD from IUT in 2016. His current research interests are in the field of intelligent piezoelectric structures and computer-aided design and engineering. **Bijan Ahmadi** graduated with a master's degree in Mechanical Engineering from the Islamic Azad University, Khomeinishahr Branch in 2017. **Sajad Hamedi** graduated with a master's degree in Mechanical Engineering from the Islamic Azad University, Khomeinishahr Branch in 2018.

Research paper

1 INTRODUCTION

The energy supply of a system from its environment is generally called energy extraction. Research in this field has attracted the attention of many engineers and researchers with the development of wireless telecommunications and the advent of low-consumption electronic devices. For example, in wireless sensor networks, the power consumption of the sensors is low enough to supply energy from the environment. Therefore, by receiving the required energy from the environment, not only is there no need for batteries and external energy sources, but due to the lack of need to charge and replace the battery, the need for special care of the system disappears, which in turn reduces costs and Environmental pollution is very effective. The growth and development of low-power electronic devices, wireless technology, and wearable and portable smart devices have led to an increase in the use of these electronic devices by individuals. These devices have facilitated our communication while requiring electrochemical batteries to supply energy. In cases of emergency personnel and field environmental research, these devices generate a significant additional load. In addition, these loads increase again due to the need to carry heavy electrochemical batteries. With the continuous development of these devices and the achievements that have been achieved in the operation of these devices, the required electrical power has also been significantly increased. However, the increase in resources is not limited to the performance of the devices, in addition, due to the limited battery life, there is still a need for constant replacement. Electrical behavior depends on centralized parameters such as resistance, capacitor, so in the simulations performed, the parameters expressing the mechanical field are considered. In 2008, Erturk and Inman [1] examined the harmonic-excited SDOF model. They showed that the conventional harmonic base excitation relationship for predicting beam motion makes large errors and showed model errors. Then they presented modifying factors to improve the SDOF model by stimulating the harmonic base in transverse and longitudinal vibrations. They determined that the SDOF model could be used for high ratios of concentrated mass to mass of beam in transverse vibration. In fact, in the case where the concentrated mass is small, there is no conventional effective mass of the cantilever beams and rods, or it produces a negligible result compared to the system response. Therefore, the proposed modified SDOF model should be used. In 2004, Sodano et al. [2] obtained a more accurate estimate than the SDOF model for the systems with distributed parameters by the Rayligh-Ritz (RR) discrete formulation. In this approach, conversion of displacements that was selected in accordance with the basic functions was used. To confirm the method, which used the Hamilton principle, they performed a laboratory study for bimorph cantilever beam with PZT material. Dutoit et al. [3] proposed an SDOF model for MEM energy harvesters. His model consisted of Euler_Bernolli beam with a concentrated mass, the Equations of which were based on the RR discretization method and the Hamilton principle and dealt with the d-31 mode. They used the piezoelectric structural relationships and the resulting electrical displacement to express the relationship between electrical output and vibrational mode shapes. Hence, a non-optimized prototype presented the power density value $30\mu\frac{W}{cm^2}$. They examined the ratio of output power to various resistance and proposed considerations for the design of piezoelectric energy harvesters, which ultimately tested the validity of the presented model by performing experiments and comparisons with previous work. However, in the 1990s, Hagood et al. [4] had used RR discretization as a modeling approach for electromechanical systems. Using Hamilton's principle, they derived coupled motion Equations for any desired elastic structure with piezoelectric and passive electronic components and developed the proposed spatial models for the output voltage of the electrodes, the direct output load of the electrodes, and the state in which the piezoelectric electrodes are indirectly connected to an arbitrary electrical circuit with built-in voltage and current sources and finally, they used these Equations for the cantilever beam. In 2006, Chen et al. [5] proposed a micro-dimensional transducer model of a piezoelectric bimorph cantilever beam that used the Hamilton principle to derive matrices of discrete mass, stiffness, and damping in the transformed space. In accordance with the base deflection approach, they formulated the relationship between voltage and induced mechanical strain. Their analytical method was based on solving with one state, and their model showed that the induced voltage is proportional to the excitation frequency and width of the piezoelectric material and is inversely proportional to the beam length and damping coefficient. They hypothesized the effect of electromechanical bonding as viscous damping. Incorporating electromechanical bonding into mechanical Equations as viscous damping coefficients is a common approach for electromagnetic harvesters [6]. But the effect of electromechanical bonding on piezoelectrics is much more complex than considering it as a viscous damping. Rafique and Bonello [7] showed that considering the effect of electromechanical bonding as a viscous damper is valid only at low resistance loads. In addition, they proved a detailed validation of the modal analysis model presented in [8] for a bimorph beam without concentrated mass around the first resonance region, validating these relationships

at frequencies higher than those considered in [8]. They investigated the effect of electromechanical bonding on the mechanical properties of the harvester, such as added resultant stiffness and damping, and by modal analysis and experiments showed that the resonant frequency and amplitude of the response due to electromechanical connection will be associated with changes. In 2013, Al-Adwani et al. [9] introduced a Shear Mode Harvester (SMH) to replace the energy harvesters in thickness mode (TMH) and longitudinal mode (LMH) in order to increase the harvested power. The reason for this choice was since the strain constant of piezoelectric material in shear is larger than the strain constant in longitudinal modes and thickness. To achieve the harvested energy in the shear mode, the piezoelectric element was polarized along a length parallel to the length of the electrode between the oscillator base and the concentrated mass. The base sinusoidal excitation in the direction of polarization causes the element to experience shear strain. They showed the optimal performance characteristics of SMH in comparison with TMH and LMH by providing numerical examples. In addition, they investigated the effect of resistance load and excitation frequency on SMH. The dynamic stiffness method relates the amplitude of the applied forces to the vibrational response of the system. This method is used to analyze systems that are harmonically excited and can provide an infinite number of natural modes for a finite number of node coordinates of continuous structures. In the present study, first, the formulas of the dynamic stiffness method are extracted, then the bimorph cantilever beam with concentrated mass at the desired distance from the end of the beam is divided into two elements and with the help of direct stiffness method, the dynamic stiffness matrix of the whole beam is obtained. This is done to damp the effect and apparent resistance in energy harvesting from the piezoelectric beam using the dynamic stiffness method.

2 THEORIES

Since common piezoelectric cantilever energy harvesters are often designed and manufactured as thin beams, and also most bimorph beams have thin structures, it seems reasonable to assume the beam as a Euler-Bernolli beam. The piezoelectric layers and the central layer are well bonded, and the electrodes that have been extended along the entire length of the beam are flexible and have a negligible thickness compared to the total thickness of the beam. In addition, the electrodes have been assumed to be well-conductive. Hence, only one electric potential difference along each electrode can be defined. Equations (1) and (2) are used to derive the behavior of moving beams with piezoelectric layers.

$$B\frac{\partial^4 u}{\partial x^4} + A\frac{\partial^5 u}{\partial x^4 \partial t} + c_a\frac{\partial u}{\partial t} + m\frac{\partial^2 u}{\partial t^2} = 0 \tag{1}$$

$$D_3 = d_{31}Y_P S + d_{31}c_P\dot{S} + \varepsilon_{33}^S E_3 \tag{2}$$

$$\begin{aligned} &\varepsilon_{33}^S = \varepsilon_{33}^T - d_{31}^2 Y_P \\ &B = Y_p I_p + Y_s I_s \\ &A = c_p I_p + c_s I_s \end{aligned} \tag{3}$$

Where S is axial strain, d_{31}, piezoelectric coefficient, E_3, Induced Electric Field, ε_{33}^T, permittivity at constant stress, D_3, component of electric displacement vector, Y_P, Modulus of elasticity of piezoelectric material, Y_S, Modulus of elasticity of the middle layer, C_P, Kelvin-Voigt damping coefficient for a piezoelectric layer, C_S, Kelvin-Voigt damping coefficient for a middle layer, I_P, the second torque of the surface around the neutral axis for a piezoelectric layer, I_S, the second torque of the surface around the neutral axis for a middle layer, m, mass per unit length, u, beam displacement in the y direction, C_a, the average viscous damping coefficient of ambience per unit length.

By placing Equation (2) in Gaussian law and deriving from it, the current intensity I as a function of time is obtained as Equation (4) where β, $C_{p'}$ and f are respectively according to Equations (5) to (7). C_p in Equation (5) is the internal capacity of a piezoelectric layer, and h_{pc} in Equation (6) is the distance from the neutral axis to the midpoint of the piezoelectric layer [10].

$$i(t) = f\beta\int_0^L \frac{\partial^3 u}{\partial x^2 \partial t}dx - \frac{f}{a}C_p\dot{v} \tag{4}$$

$$\beta = -\mathrm{d}_{31}\mathrm{Y}_\mathrm{p}\mathrm{h}_{\mathrm{pc}}\mathrm{b} \tag{5}$$

$$C_p = \varepsilon_{33}^S\frac{bL}{h_p} \tag{6}$$

$$f = \begin{cases} 1, & for\ series \\ 2, & for\ parallel \end{cases} \tag{7}$$

h_p is the thickness of a piezoelectric layer, $v(t)$ is the voltage of the whole set is equal to 2 and 1 for series and parallel, respectively, L is the length, and b is the width of the beam.

For dynamic stiffness analysis, harmonic excitation is assumed. Hence, the displacement is obtained from Equations (3-30). Using the Equations (8) and (10), Equation (10) would be achieved [11].

$$u(x,t) = \tilde{u}(x)e^{j\omega t} \tag{8}$$

$$B(e^{j\omega t})\left(\frac{\partial^4\tilde{u}}{\partial x^4}\right)+A(j\omega)(e^{j\omega t})\left(\frac{\partial^4\tilde{u}}{\partial x^4}\right)+c_a(j\omega)e^{j\omega t}\tilde{u}+m(j\omega)^2e^{j\omega t}\tilde{u}=0 \quad (9)$$

$$\tilde{u}^{iv}-k\tilde{u}=0 \quad (10)$$

$$k=\omega^{\frac{1}{2}}\left[\frac{m}{\hat{B}/\left(1-j\frac{c_a}{m\omega}\right)}\right]^{\frac{1}{4}} \quad (11)$$

$$\hat{B}=B\left(1+j\omega\frac{A}{B}\right) \quad (12)$$

Because the excitation is harmonic, parameters such as M (x, t), Q (x, t), θ (x, t) and v (t) are in the form of (13) Equations.

$$M(x,t)=\tilde{M}(x)\,e^{j\omega t}\quad Q(x,t)=\tilde{Q}(x)\,e^{j\omega t}\quad \theta(x,t)=\tilde{\theta}(x)\cos e^{\,j\omega t}\quad v(t)=\tilde{v}\,e^{j\omega t}\quad i(t)=\tilde{\imath}\,e^{j\omega t} \quad (13)$$

Using Equations (9), (12) and (4), the bending moment amplitude is obtained from (14) Equation [12].

$$\tilde{M}(x)=\hat{B}\,\tilde{u}''+\vartheta\tilde{v}\quad \tilde{Q}(x)=\hat{B}\tilde{u}''' \quad (14)$$

If Z is the symbol of the apparent resistance of the electric charge, Equation (15) can be written. By placing (15) in (4), the voltage amplitude would be achieved by Equation (16), in which G can be obtained in Equation (17) [13].

$$\tilde{v}=Z\tilde{\imath} \quad (15)$$

$$\tilde{v}=G\left[\tilde{\theta}(L)-\tilde{\theta}(O)\right] \quad (16)$$

$$G=\frac{j\omega f\beta}{j\omega\left(\frac{f}{a}\right)C_p+\frac{1}{Z}} \quad (17)$$

The dynamic stiffness matrix of the beam with the concentrated mass shown in "Fig. 3" can be determined by calculating relations (18) [14].

$$\mathrm{f}=\mathrm{Du}\qquad \mathrm{f}=\left[\tilde{F}_0\ \tilde{\Gamma}_0\ \ \tilde{F}_L\ \tilde{\Gamma}_L\right]^T\qquad \mathrm{u}=\left[\tilde{u}_0\ \tilde{\theta}_0\ \ \tilde{u}_L\ \tilde{\theta}_L\right]^T \quad (18)$$

It should be noted that the dimensions of the concentrated mass are assumed in comparison with the dimensions of the previous beam, therefore, the displacement of the end of the beam and the concentrated mass will be the same. also the moment of inertia of the concentrated mass is neglected. Hence, according to "Fig. 1", relation (19) is written in which f_e corresponds to relation (18) [15].

$$\mathrm{f_e}=\mathrm{D_e u}\qquad \mathrm{f_e}=\left[\tilde{F}_0\ \tilde{\Gamma}_0\ \ \tilde{F}_{L_e}\ \tilde{\Gamma}_{L_e}\right]^T \quad (19)$$

From "Fig. 1", the boundary conditions are obtained as Equations (20).

$$\tilde{M}(O)=-\tilde{\Gamma}_0\quad \tilde{M}(L)=\tilde{\Gamma}_{L_e}\quad \tilde{Q}(O)=\tilde{F}_0\quad \tilde{Q}(L)=-\tilde{F}_{L_e} \quad (20)$$

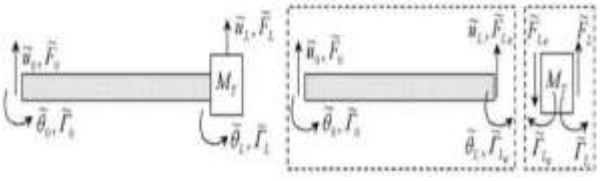

Fig. 1 Free body diagram of the beam with a concentrated mass (The damping forces are not displayed).

As a result, Equation (21) would be achieved by solving Equation (14) [16]. By applying the boundary conditions and Equation (21) in Equations (18) and (19), relations (22) to (25) are obtained.

$$\tilde{u}(x)=C_1\cosh kx+C_2\sinh kx+C_3\cos kx+C_4\sin kx \quad (21)$$

$$\tilde{\Gamma}_0=\hat{B}k^2(-C_1+C_3)+\vartheta G\left(\tilde{\theta}_0-\tilde{\theta}_L\right) \quad (22)$$

$$\tilde{\Gamma}_{L_e}=\hat{B}k^2(C_1\cosh kL+C_2\sinh kL-C_3\cos kL-C_4\sin kL)+\vartheta G\left(\tilde{\theta}_L-\tilde{\theta}_0\right) \quad (23)$$

$$\tilde{F}_0=\hat{B}k^3(C_2-C_4) \quad (24)$$

$$\tilde{F}_{L_e}=\hat{B}k^3(-C_2\cosh kL-C_1\sinh kL+C_4\cos kL-C_3\sin kL) \quad (25)$$

The relations from (22) to (25) can be written in matrix form as Equation (26).

$$\begin{bmatrix}\tilde{F}_0\\ \tilde{\Gamma}_0\\ \tilde{F}_{L_e}\\ \tilde{\Gamma}_{L_e}\end{bmatrix} = \vartheta G \begin{bmatrix}0 & 0 & 0 & 0\\ 0 & 1 & 0 & -1\\ 0 & 0 & 0 & 0\\ 0 & -1 & 0 & 1\end{bmatrix}\begin{bmatrix}\tilde{u}_0\\ \tilde{\theta}_0\\ \tilde{u}_L\\ \tilde{\theta}_L\end{bmatrix} + \hat{B}k^2 \begin{bmatrix}0 & k & 0 & -k\\ -1 & 0 & 1 & 0\\ -k\sinh kL & -k\cosh kL & -k\sin kL & k\cos kL\\ \cosh kL & \sinh kL & -\cos kL & -\sin kL\end{bmatrix}\begin{bmatrix}C_1\\ C_2\\ C_3\\ C_4\end{bmatrix} \quad (26)$$

The relation (27) is obtained by computing the derivative of Equation (21). Hence, $\tilde{u}$ and $\tilde{\theta}$ at the beginning and end of the beam will be according to the relations (28) to (31), which are written in matrix form as Equation (3-65). u and C are also according to Equations (32) and (33).

$$\tilde{\theta}(x) = k\,(C_1\sinh kx + C_2\cosh kx - C_3\sin kx + C_4\cos kx) \quad (27)$$

$$\tilde{u}_0 = C_1 + C_3 \quad (28)$$

$$\tilde{\theta}_0 = k(C_2 + C_4) \quad (29)$$

$$\tilde{u}_L = C_1\cosh kL + C_2\sinh kL + C_3\cos kL + C_4\sin kL \quad (30)$$

$$\tilde{\theta}_L = k(C_1\sinh kL + C_2\cosh kL - C_3\sin kL + C_4\cos kL) \quad (31)$$

$$\mathrm{u} = \mathrm{AC} \qquad \mathrm{C} = [C_1 \quad C_2 \quad C_3 \quad C_4] \quad (32)$$

$$\mathrm{A} = \begin{bmatrix}1 & 0 & 1 & 0\\ 0 & k & 0 & k\\ \cosh kL & \sinh kL & \cos kL & \sin kL\\ k\sinh kL & k\cosh kL & -k\sin kL & k\cos kL\end{bmatrix} \quad (33)$$

To obtain f_e as a function of u, C from (30) is placed in Equation (24). If C is placed from Equation (30) to Equation (24), the dynamic stiffness matrix of the beam is obtained using the above relations as Equation (34), in which D_e is known as the dynamic stiffness matrix of the Beam without electric coupling and can be achieved in short circuit conditions [17].

$$\mathrm{D_e} = \begin{bmatrix}S_1 & S_2 & S_3 & S_4\\ S_2 & S_5 & -S_4 & S_6\\ S_3 & -S_4 & S_1 & -S_2\\ S_4 & S_6 & -S_2 & S_5\end{bmatrix} + \vartheta G \begin{bmatrix}0 & 0 & 0 & 0\\ 0 & 1 & 0 & -1\\ 0 & 0 & 0 & 0\\ 0 & -1 & 0 & 1\end{bmatrix} \quad (34)$$

$$S_1 = \frac{\hat{B}k^3(\cos kL\,.\sinh kL + \cosh kL\,.\sin kL)}{\Delta}$$

$$S_2 = \frac{\hat{B}k^2(\sin kL\,.\sinh kL)}{\Delta}$$

$$S_3 = -\frac{\hat{B}k^3(\sin kL + \sinh kL)}{\Delta}$$

$$S_4 = \frac{\hat{B}k^2(\cosh kL - \cos kL)}{\Delta}$$

$$S_5 = \hat{B}k\frac{(\cosh kL\,.\sin kL - \cos kL\,.\sinh kL)}{\Delta}$$

$$S_6 = \hat{B}k\frac{(\sinh kL - \sin kL)}{\Delta}$$

According to "Fig. 2", which shows the free diagram of the concentrated mass, the relations (35) and (36) can be written. In these two relations, M_T represents the concentrated mass, and I_T represents the moment of inertia of the concentrated mass. In Equation (35), C_T indicates the ambient damping coefficient per concentrated mass and is considered as Equation (37) in order to compare the dynamic stiffness method with modal analysis [18].

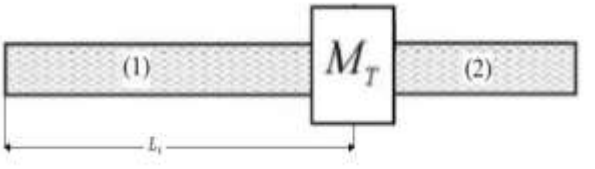

Fig. 2 Bimorph beam with concentrated mass at a distance of L_i from the base of the beam.

$$F_L - F_{L_e} = M_T\ddot{u}_L + c_T\dot{u} \quad (35)$$

$$\Gamma_L - \Gamma_{L_e} = I_T\ddot{\theta}_L \quad (36)$$

$$c_T = c_a\frac{M_T}{m} \quad (37)$$

Equations (38) and (39) would be achieved, if $e^{i\omega t}$ is removed from relations (35) and (36). Also, if Equation (13) is subtracted from (10), the relation (40) is obtained.

$$\tilde{F}_L - \tilde{F}_{L_e} = -\omega^2 M_T\,\tilde{u}_L + j\omega c_a\frac{M_T}{m}\tilde{u}_L \quad (38)$$

$$\tilde{\Gamma}_L - \tilde{\Gamma}_{L_e} = -\omega^2 I_T\,\tilde{\theta}_L \quad (39)$$

$$\mathrm{f} - \mathrm{f_e} = (\mathrm{D} - \mathrm{D_e})\mathrm{u} \quad (40)$$

By placing the relations (38) and (39) in (40), Equation (41) is written. Hence, by using relation (41), Equation (42) is obtained in which D_m corresponds to Equation (43) [19].

$$\begin{bmatrix} \tilde{F}_0 - \tilde{F}_0 \\ \tilde{\Gamma}_0 - \tilde{\Gamma}_0 \\ \tilde{F}_L - \tilde{F}_{L_e} \\ \tilde{\Gamma}_L - \tilde{\Gamma}_{L_e} \end{bmatrix} = \begin{bmatrix} 0 & 0 & 0 & 0 \\ 0 & 0 & 0 & 0 \\ 0 & 0 & -\omega^2 M_T - j\omega c_a \frac{M_T}{m} & 0 \\ 0 & 0 & 0 & -\omega^2 I_T \end{bmatrix} \begin{bmatrix} \tilde{u}_0 \\ \tilde{\theta}_0 \\ \tilde{u}_L \\ \tilde{\theta}_L \end{bmatrix} \quad (41)$$

$$D = D_e + \begin{bmatrix} 0 & 0 \\ 0 & D_m \end{bmatrix} \quad (42)$$

$$D_m = \begin{bmatrix} -\omega^2 M_T + j\omega c_a \frac{M_T}{m} & 0 \\ 0 & -\omega^2 I_T \end{bmatrix} \quad (43)$$

The matrix R is defined as relation (44), therefore, u is obtained according to relation (45) [18].

$$R = D^{-1} \quad (34)$$

$$u = Rf \quad (45)$$

Given that there is no external excitation on the concentrated mass, Equation (45) can be extended to Equation (46).

$$\begin{bmatrix} \tilde{u}_0 \\ \tilde{\theta}_0 \\ \tilde{u}_L \\ \tilde{\theta}_L \end{bmatrix} = \begin{bmatrix} R_{11} & R_{12} & R_{13} & R_{14} \\ R_{21} & R_{22} & R_{23} & R_{24} \\ R_{31} & R_{32} & R_{33} & R_{34} \\ R_{41} & R_{42} & R_{43} & R_{44} \end{bmatrix} \begin{bmatrix} \tilde{F}_0 \\ \tilde{\Gamma}_0 \\ 0 \\ 0 \end{bmatrix} \quad (46)$$

Using the presented relations, the output voltage is obtained as in Equation (47) [20]. Also, the output displacement as Equation (48) can be achieved by placing relations (46) and (47) in Equation (46) [20].

$$\tilde{v} = G\left[\frac{R_{41}R_{22} - R_{42}R_{21}}{\alpha}\right]\tilde{u}_0 + G\left[\frac{R_{42}R_{11} - R_{41}R_{12} - \alpha}{\alpha}\right]\tilde{\theta}_0 \quad (47)$$

$$\tilde{u}_L = \left(\frac{R_{31}R_{22} - R_{32}R_{21}}{\alpha}\right)\tilde{u}_0 + \left(\frac{R_{32}R_{11} - R_{31}R_{12}}{\alpha}\right)\tilde{\theta}_0 \quad (48)$$

Given that the sample beam is of the bimorph type, the relations related to the bimorph beam are extracted. The purpose of this work is to convert the beam into two arbitrary elements and to obtain the effect of concentrated mass displacement on the system. To obtain the output voltage of the system, Gauss's law for a piezoelectric layer is written as Equation (49).

$$q = -\int_o^L yY_p d_{31} \frac{b\partial^2 u}{\partial x^2} dx + \int_o^L b\varepsilon_{33}^S E_3 dx \quad (49)$$

Because the electrodes are completely conductive and the electrical potential is the same throughout the electrode, the amount of charge accumulated in the middle section of the top layer is obtained according to relation (50). Hence, by computing the derivative of Equation (50) with respect to time, the intensity of electric current through the external resistance will be under Equation (51) for a piezoelectric layer.

$$q = -h_{pc}Y_p d_{31} \int_o^L b\frac{\partial^2 u}{\partial x^2} dx - \frac{\varepsilon_{33}^S v(t)}{h_p}\int_o^L b dx \quad (50)$$

$$i(t) = -h_{pc}Y_p d_{31} \int_o^L b\frac{\partial^3 u}{\partial x^2 \partial t} dx - \frac{\varepsilon_{33}^S \dot{v}(t)}{h_p}\int_0^L b dx \quad (51)$$

Equation (52) represents the current flowing through the apparent resistance for the whole system in series and parallel connection. Assuming the excitation of the system is harmonic, the output voltage amplitude is written according to relation (53).

$$i(t) = -h_{pc}Y_p d_{31} f \int_0^L b\frac{\partial^3 u}{\partial x^2 \partial t} dx - \frac{f\varepsilon_{33}^S \dot{v}(t)}{a h_p}\int_0^L b dx \quad (52)$$

$$\tilde{v} = \left[\frac{-j\omega h_{pc}Y_p d_{31}}{\frac{-j\omega\varepsilon_{33}^S}{h_p}(\frac{f}{a})\int_0^L b dx + \frac{1}{Z}}\right]\int_o^L bu'' dx \quad (53)$$

Equation (53) can be used for beams of uniform thickness with the number of arbitrary elements and different cross sections, but for the system shown in "Fig. 2", the voltage amplitude is obtained as Equation (54) in which $\tilde{\theta}_{L_i}^{(2)} and\ \tilde{\theta}_{L_i}^{(1)}$ are slope range in L_i for element 1 and element 2, respectively.

$$\tilde{v} = G\left[\tilde{\theta}_L - \tilde{\theta}_{L_i}^{(2)} + \tilde{\theta}_{L_i}^{(1)} - \tilde{\theta}_0\right] \quad (54)$$

Due to the continuity of the beam and the concentration of the mass, $\tilde{\theta}_{Li}^{(1)}$ and $\tilde{\theta}_{Li}^{(2)}$ are equal and the voltage amplitude is obtained according to Equation (27). Again, it is observed that the output voltage depends only on the beginning and end slopes of the beam and is independent of $\tilde{\theta}_{Li}$. This is because the width of the beam is uniform, but if the value of b changes at L_i then the output voltage will depend on the slope at the point L_i.

$$\tilde{v} = G\left[\tilde{\theta}_L - \tilde{\theta}_o\right] \quad (55)$$

If D_1 and D_2 are the dynamic stiffness matrices of element 1 and element 2 in "Fig. 2", respectively, the dynamic stiffness matrix of the whole system can be obtained by the direct stiffness method, in which the relations (56) to (58) are written for the whole system.

$$f = Du \tag{56}$$

$$u = \left[\tilde{u}_0 \;\; \tilde{\theta}_0 \;\; \tilde{u}_{L_i} \;\; \tilde{\theta}_{L_i} \;\; \tilde{u}_L \;\; \tilde{\theta}_L\right] \tag{57}$$

$$f = \left[\tilde{F}_0 \;\; \tilde{\Gamma}_0 \;\; \tilde{F}_{L_i} \tilde{\Gamma}_{L_i} \;\; \tilde{F}_L \;\; \tilde{\Gamma}_L \;\; \right] \tag{58}$$

Due to the lack of external excitation at points L and L_i, the values of external force and torque are equal to zero, hence by considering Equation (47), the voltage amplitude and displacement range of the end of the beam will be obtained by Equations (59) and (60) as a function of $\tilde{u}_0$ and $\tilde{\theta}_0$.

$$\tilde{v} = G\left[\frac{R_{61}\,R_{22}-R_{62}R_{21}}{\alpha}\right]\tilde{u}_0 + G\left(\frac{R_{62}\,R_{11}-R_{61}\,R_{12}-\alpha}{\alpha}\right)\tilde{\theta}_0 \tag{59}$$

$$\tilde{u}_L = \left(\frac{R_{51}\,R_{22}-R_{52}\,R_{21}}{\alpha}\right)\tilde{u}_0 + \left(\frac{R_{52}\,R_{11}-R_{51}\,R_{22}}{\alpha}\right)\tilde{\theta}_0 \tag{60}$$

3 SAMPLE SPECIFICATIONS AND RESULTS

The system is analyzed with the specifications given in "Table 1". Also, the damping ratios for the first two modes are $\zeta_1 = 0.0166$ and $\zeta_2 = 0.0107$, respectively, and the amount of concentrated mass (M_T) is equal to $0.5m_b$ [21]. By using the values ζ_1 and ζ_2 that are presented for two modes, and also Equation (60), the values C_a and A can be achieved. The values ζ_3 and ζ_4 are obtained by using the values ζ_1 and ζ_2, although it may not be valid for the higher modes of C_a and A [1].

Table 1 Dimensions and mechanical and physical properties of the system

h_p (mm)	0.267	L (mm)	60
h_s (mm)	0.300	(kg/m^3) Piezoelectric layer density	7800
Y_p (GPa)	6200	(kg/m^3) middle layer density	2700
Y_S (GPa)	7200	d_{31} (m/V)	-320×10^{-12}
b (mm)	25	ε_{33}^{T} $(\frac{F}{m})$	3.3646×10^{-8}

Because the maximum ratio of output voltage to base acceleration for a distance of 38 mm mass from the base occurs at the first resonant frequency, and at the second resonant frequency, the maximum ratio of output voltage to base acceleration for concentrated mass is obtained in 16 mm, the effect of Kelvin-Voigt damping coefficients and viscous damping for these two concentrated mass locations is investigated. For this purpose, the FRFs of voltage to base acceleration ratio are plotted for several A / B values and compared with the undamped mode ("Fig. 3").

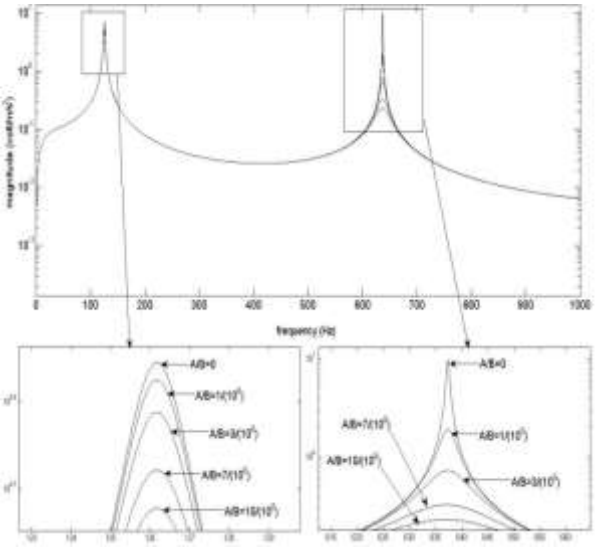

Fig. 3 The FRF of output voltage to base acceleration ratio to rise A/B values.

As shown in "Fig. 3", despite the small A/B values, changing it greatly affects the system output. This effect on the output voltage to the base acceleration ratio at the second resonant frequency is greater, so that this decline has been 97.61% for changing the value of A / B from 0 to 10×10^{-6}, but at first resonant frequency, it dropped to 31.97% for changing the value of A / B from 0 to 10×10^{-6}. In the undamped mode for concentrated mass with 16 mm far from the base, the voltage to base acceleration ratio at the second resonant frequency is greater than this value at the first resonant frequency, but gradually with the growth of the value A/B due to the fact that the rise of damping at the second resonant frequency causes that the voltage falls considerably, the output voltage to base acceleration ratio at the first resonant frequency compared to this value in the second resonant frequency is remarkable. As far as A / B is equal to $6 \times 10 \times 10^{-6}$, the proportion of output voltage to base acceleration at the first resonant frequency is 4.76 volt/ m and at the second resonant frequency is 0.2314 volt/ m ("Fig. 4").

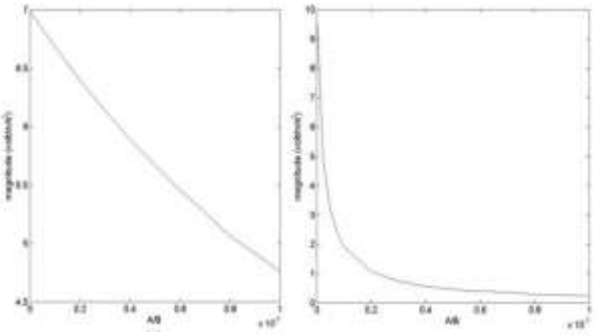

(b) **(a)**

Fig. 4 (a): The ratio of output voltage to base acceleration at the second resonant frequency in accordance with A/B changes, and (b): The ratio of output voltage to base acceleration at the first resonant frequency in accordance with A/B changes.

As can be seen in "Fig. 4", the decline in output voltage at the first resonant frequency occurs due to the growth of damping with a gentle slope and almost linearly, but at the second resonant frequency this drop was initially abrupt, then the effect of growth of this damping on the system output will be dropped by rising the A/B. The diagrams in "Fig. 4" are drawn based on A/B variations. These changes for $\omega_{r_1} = 126.21$ Hz and $\omega_{r_2} = 637.4$ Hz are equal to $0.004 < \zeta_1 < 0$ and $0.02 < \zeta_2 < 0$. For this reason, a marked drop in voltage at the second resonant frequency can be justified. For the concentrated mass with 38 mm far from the base, the effect of A/B changes is shown in "Fig. 5".

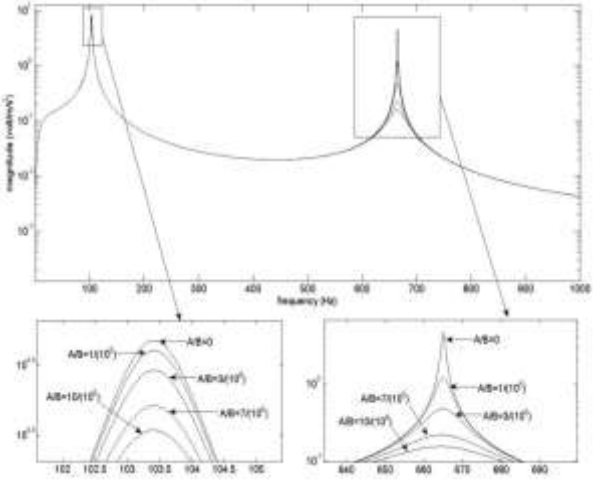

Fig. 5 The ratio of output voltage to base acceleration based on excitation frequency to raise the values A/B 38.

As in "Fig. 3", the effect of the A/B changes for the second resonant frequency on the graph is very high, but this decline occurs at the first resonant frequency with a gentle slope and almost linearly ("Fig. 6").

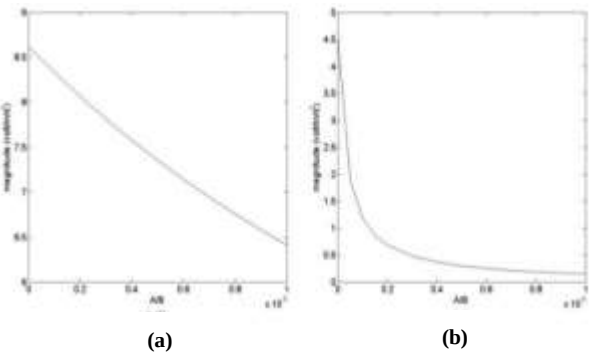

(a) **(b)**

Fig. 6 (a): The ratio of output voltage to base acceleration at the first resonant frequency in accordance with A/B changes for 38, and (b): The ratio of output voltage to base acceleration at the second resonant frequency in accordance with A / B changes for 38.

For the concentrated mass with 38 mm far from the base, the proportion of voltage to base acceleration from the second resonant frequency is less than this ratio at the first resonant frequency in which by changes of A/B, it would decline to 96.5% and 25.65%, respectively. It should be noted that this range of changes for A / B is equal to $0 < \zeta_1 < 0.0032$ and $0 < \zeta_2 < 0.0209$.

The FRFs of voltage to base acceleration ratio for various values of C_a/m for a system with concentrated mass and a distance of 16 mm are according to "Fig. 7".

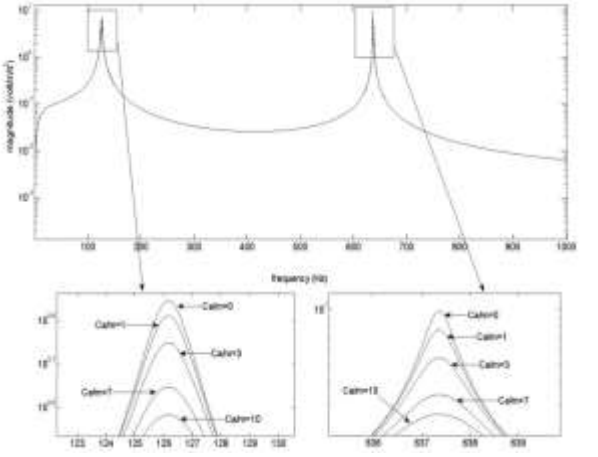

Fig. 7 The ratio of output voltage to base acceleration based on excitation frequency to raise the values C_a/m.

Unlike Kelvin-White damping, the changes of viscous damping upon the reduction of the voltage-to-acceleration ratio for the first and second resonant frequencies follow almost the same pattern ("Fig. 8"). However, the graph changes for the second resonant frequency are greater than the first resonant frequency, so that this decline is 72.66% and 45.19%, respectively.

The range of changes from 0 to 10 for C_a / m is equal to $0 < \zeta_1 < 0.0063$ and $0 < \zeta_2 < 0.0012$.

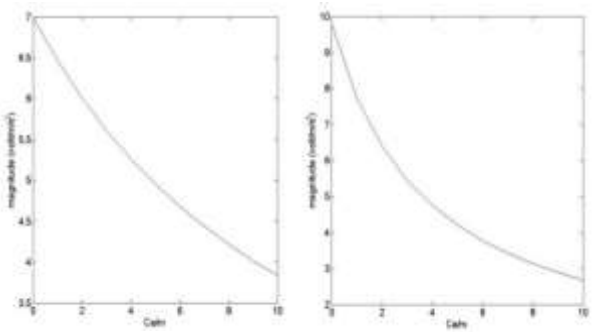

(a) **(b)**

Fig. 8 (a): The ratio of output voltage to base acceleration at the first resonant frequency in accordance with C_a/m changes for 16, and (b): The ratio of output voltage to base acceleration at the second resonant frequency in accordance with C_a/m changes for 16.

For a system with a concentrated mass at a distance of 38 mm from the base, the FRFs of the voltage to base acceleration ratio have been drawn ("Fig. 9").

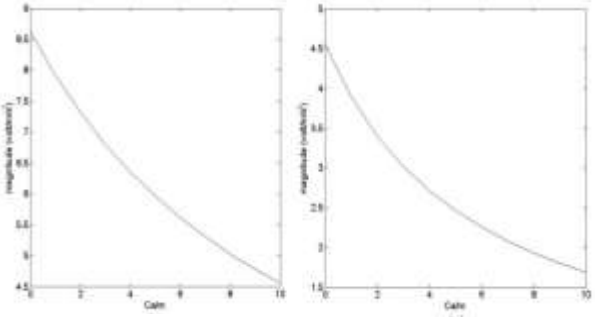

(a) **(b)**

Fig. 9 (a): The ratio of output voltage to base acceleration at the first resonant frequency in accordance with C_a / m changes for 38, and (b): The ratio of output voltage to base acceleration at the second resonant frequency in accordance with C_a / m changes for 38.

Similar to what happens for the concentrated mass at a distance of 16 mm due to the change in C_a/m, the reduction in diagrams 4-16 a and b is almost the same, and this decline is greater at the second resonant frequency. This drop for the first and second resonant frequencies is 47.20% and 62.95%, respectively. The range of changes from 0 to 10 for C_a / m is equal to $0 < \zeta_1 < 0.0077$ and $0 < \zeta_2 < 0.0012$. As a result, it can be said that a little growth in A/B from the undamped mode causes a sharp drop in the proportion of voltage to base acceleration for the second resonant frequency, although it should be noted that this decline would be gentle for the first resonant frequency. The reason is that the rise of A/B causes the greater growth of ζ_r for the next modes of the system. Therefore, one of the factors that reduces the effect of the system response in the resonant frequencies is Kelvin-Voigt damping. Regarding the effect of viscous damping, it should be said that the rise of C_a/m causes less growth in ζ_r for higher modes of the system. Despite this, the decline in the second resonant frequency is greater than the decline in the first resonant frequency, which, unlike Kelvin-Voigt damping, does not cause a sudden reduction in system output due to the rise of damping frequency in the second resonant frequency and occurs gently. Therefore, because the proportion of the voltage to acceleration drops sharply due to the rise of Kelvin-Voigt damping coefficients in the second resonant frequency, the best place for energy harvesting is where the concentrated mass is 38mm away from the base.

According to the analysis performed in the previous section, a system with a concentrated mass that is 38 mm away from the base was proposed. Therefore, this system is used to investigate the effect of apparent resistance. In addition, it is assumed that the qualification factors remain constant due to the displacement of the concentrated mass, according to which the relations C_a/m = 7.71934 and A/B= 8.5000198×10^{-6} are established. The output power for the system changes with the alteration of the apparent resistance. These changes have been drawn for a resistor R of 10 Ω, which is very close to the short circuit conditions ("Figs. 4-12"). The harvested voltage rises with increasing R to reach its maximum in open-circuit mode. The effect of increasing the apparent resistance ("Fig. 10") on the portability of the beam tip relative to the base is such that as the apparent resistance rises, its natural frequencies grow, hence making the system more rigid [22].

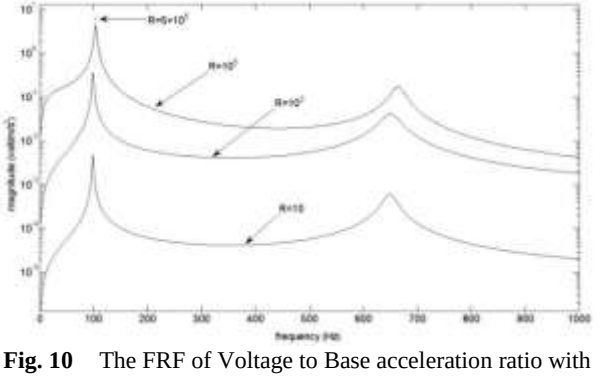

Fig. 10 The FRF of Voltage to Base acceleration ratio with rise of apparent resistance in ohms from short circuit to open circuit mode.

Increasing the apparent resistance from 10^3 Ω to 10^5 Ω raises the natural first and second frequencies by 5.04% and 2.19%. The growth in natural frequencies can be neglected by raising the apparent resistance from 10^5 Ω to 5×10^5 Ω. It should be noted that the frequency of

the peaks of the transmittable diagram overlaps the FRF frequency of the voltage-to-base acceleration ratio.

In some cases, the net load of the capacitor is expressed as $Z = 1 / j\omega C$ in which the capacitance of the capacitor is $C = nC_p$. The transmissibility diagram of the beam tip relative to the beam base is drawn to rise the values of n:

$n = 0$ is equivalent to the open circuit conditions, $n = \infty$ is equivalent to the short circuit state, and $n = 10^{-4}$ is considered when experimental open circuit conditions are in place [23]. A comparison of "Figs. 11 and 12" shows that the system becomes more rigid as the conditions change from short circuit to open circuit, but the reduction in the amplitude of the diagram is negligible.

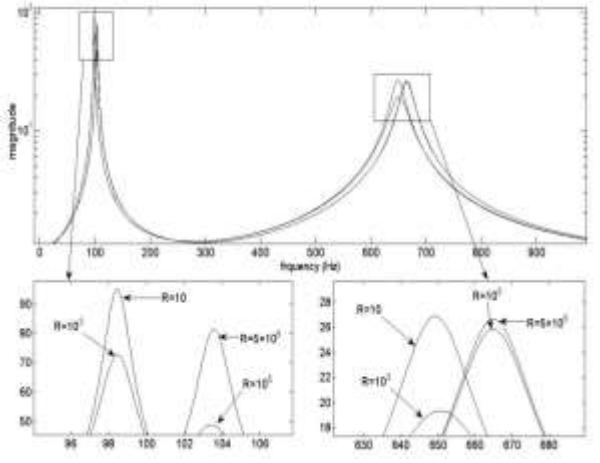

Fig. 11 Transmissibility of the beam tip relative to the beam base to raise the apparent resistance values ohms from the short circuit state to the open circuit state.

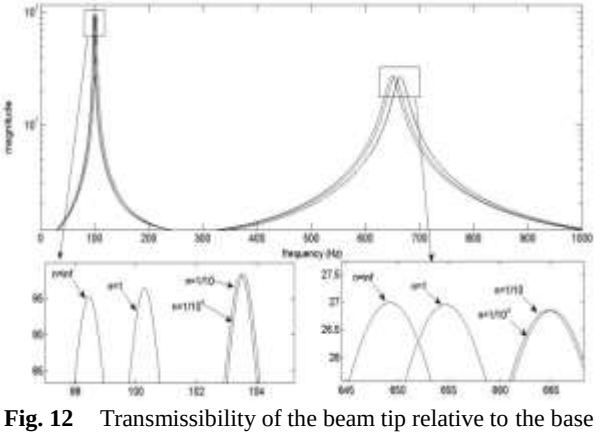

Fig. 12 Transmissibility of the beam tip relative to the base beam in accordance with changes in various values of capacitor load.

4 CONCLUSIONS

In this study, a dynamic stiffness method was developed to harvest energy from a piezoelectric beam despite damping and apparent resistance with concentrated mass. The intended purpose is to investigate the effect of damping and apparent resistance on energy harvesting from piezoelectric beams using the dynamic stiffness method. According to the results obtained in this study, changes in Kelvin-Voigt damping coefficients and viscous damping were investigated in which with rising the Kelvin-Voigt damping coefficient from undamped mode, the proportion of voltage amplitude to base acceleration in the second resonant frequency dropped sharply, but with further growth of this coefficient, the amplitude declined with a gentle slope. A reduction in FRF of voltage to acceleration ratio at the first resonant frequency occurred almost linearly with a gentle slope due to the rise in Kelvin-Voigt damping. The effect of rising the viscous damping on the FRF amplitude of voltage to base acceleration ratio in the first resonant frequency resembled the changes in the Kelvin-Voigt damping coefficient, however the effect of this coefficient on decreasing the amplitude of the diagram in the second resonant frequency was not as severely as before and was almost close to decline of the diagram amplitude in the first resonant frequency.

Regarding the effect of damping coefficients for the maximum output voltage harvesting, a system was proposed whose concentrated mass was 38 mm away from the base, and the effect of apparent resistance and capacitor load on the transmissibility of the beam tip relative to the base was investigated for this system. As a result of raising the resistance load from the short circuit to open circuit conditions, the natural frequencies of the system became more magnified. In fact, raising the resistance load made the system more rigid. A similar change in the system's natural frequencies occurred from short circuit to open circuit conditions to change the capacitor load. It should be noted that the reduction in the FRF of the Voltage to acceleration ratio was significant in the resistance load alteration, although the reduction of this amplitude in changing the capacitor load could be ignored. Given that the dynamic stiffness matrix of the beam element was obtained with a uniform cross section and concentrated mass, the element matrix can be used to analyze the set of interconnected beams. Also, a trapezoidal beam can be divided into different parts, and the dynamic stiffness matrix of each segment can be calculated separately. Finally, by assembling the stiffness matrices of the elements by the direct stiffness method, the electrical output for this beam can be obtained. The DSM method can be used for a variety of boundary conditions, so obtaining electrical outputs for different boundary conditions can be deliberated.

REFERENCES

[1] Erturk, A., Inman, D. J., On Mechanical Modeling of Cantilevered Piezoelectric Vibration Energy Harvesters, J. Intell. Mater. Syst. Struct., Vol. 19, 2008, pp. 1311-1325.

[2] Sodano, H. A., Park, G., and Inman, D. J., Estimation of Electric Charge Output for Piezoelectric Energy Harvesting, Strain, Vol. 40, 2004, pp. 49-58.

[3] DuToit, N. E., Wardle, B. L., and Kim, S. G., Design Considerations for MEMs-Scale Piezoelectric Mechanical Vibration Energy Harvesters, Integrated Ferroelectrics, Vol. 71, 2005, pp. 121–160.

[4] Hagood, N. W., Chung, W. H., and Von Flotow, A., Modelling of Piezoelectric Actuator Dynamics for Active Structural Control, J. Intell. Mater. Syst. and Struct., 1990.

[5] Chen, S. N., Wang, G. J., and Chien, M. C., Analytical Modeling of Piezoelectric Vibration-Induced Micro Power Generator, Mechatronics, Vol. 16, 2006, pp. 379-387.

[6] Williams, C. B., Yates, R. B., Analysis of a Micro-Electric Generator for Microsystems, Sensors and Actuators A, Vol. 52, 1996, pp. 8-11.

[7] Rafique, S., Bonello, P., Experimental Validation of a Distributed Parameter Piezoelectric Bimorph Cantilever Energy Harvester, Smart Mater. Struct., Vol. 19, 2010, pp. 094008.

[8] Erturk, A., Inman, D. J., A Distributed Parameter Electromechanical Model for Cantilevered Piezoelectric Energy Harvesters, ASME J. Vibr. Acoust., Vol. 130, 2008, pp. 041002.

[9] Aladwani, A., Aldraihem, O., and Baz, A., Single Degree of Freedom Shear-Mode Piezoelectric Energy Harvester, ASME J. Vibr. Acoust., Vol. 135, 2013, pp. 051011.

[10] Bonello, P., Rafique, S., J., Modeling and Analysis of Piezoelectric Energy Harvesting Beams Using the Dynamic Stiffness and Analytical Modal Analysis Methods, ASME J. Vibr. Acoust., Vol. 133, 2011, pp. 011009.

[11] Banerjee, J. R., Sobey, A. J., Dynamic Stiffness Formulation and Free Vibration Analysis of A Three-Layered Sandwich Beam, International Journal of Solids and Structures, Vol. 42, 2005, pp. 2181–2197.

[12] Banerjee, J. R., Cheung, C. W., Morishima, R., Perera, M., and Njuguna, J., Free Vibration of A Three-Layered Sandwich Beam Using the Dynamic Stiffness Method and Experimen, International Journal of Solids and Structures, Vol. 44, 2007, pp. 7543–7563.

[13] Khalili S. M. R., Nemati N., Malekzadeh, K., and Damanpack, A. R., Free Vibration Analysis of Sandwich Beams Using Improved Dynamic Stiffness Method, Composite Structures, Vol. 92, 2010, pp. 387–394.

[14] Damanpack, A. R., Khalili, S. M. R., High-Order Free Vibration Analysis of Sandwich Beams with A flexible Core Using Dynamic Stiffness Method, Composite Structures, Vol. 94, 2012, pp. 1503–1514.

[15] Jafari, M., Mahjoob, M. J., An Exact Three-Dimensional Beam Element With Nonuniform Cross Section, School of Mechanical Engineering, Vol. 77, 2010, pp. 61–72.

[16] Ratazzi, A. R., Bambill, D. V., and Rossit, C. A., Free Vibrations of Beam System Structures with Elastic Boundary Conditions and an Internal Elastic Hinge, Chinese Journal of Engineering, Vol. 89, 2013, pp. 556–568.

[17] Su, H., Banerjee, J. R., Development of Dynamic Stiffness Method for Free Vibration of Functionally Graded Timoshenko Beams, Computers and Structures, Vol. 147, 2015, pp. 107–116.

[18] Jeon, Y. B., Sood, R., Jeong, J. H., and Kim, S. G., MEMS Power Generator with Transverse Mode Thin Film PZT, Sensors and Actuators A, Vol. 122 2005, pp. 16–22.

[19] Erturk, A., Inman, D. J., An Experimentally Validated Bimorph Cantilever Model for Piezoelectric Energy Harvesting From Base Excitations, Smart Mater. Struct., Vol. 18, 2009, pp. 79–88.

[20] Leung, Y. T., Dynamic Stiffness Method for Exponentially Varying Harmonic Excitation of Continuous Systems, Journal of Sound and Vibration, Vol. 98, No. 3, 1985, pp. 337-347.

[21] Lin, J. H., Wu, X. M., Ren, T. L., and Liu, L. T., Modeling and Simulation of Piezoelectric MEMS Energy Harvesting Device, Integrated Ferroelectrics, Vol. 95, 2007, pp. 128–141.

[22] Kim, J. E., Kim, Y. Y., Analysis of Piezoelectric Energy Harvesters of a Moderate Aspect Ratio With a Distributed Tip Mass, Journal of Vibration and Acoustics, Vol. 115, 2011, pp. 178–194.

[23] Aladwani, A., Arafa, M., Aldraihem, O., and Baz, A., Cantilevered Piezoelectric Energy Harvester With a Dynamic Magnifier, ASME J. Vibr. Acoust., Vol. 134, 2012, pp. 031004.